Materials Science & Engineering C 84 (2018) 208–217

Contents lists available at ScienceDirect

Materials Science & Engineering C

journal homepage: www.elsevier.com/locate/msec

Gold-capped silicon for ultrasensitive SERS-biosensing: Towards human biofluids analysis

Agnieszka Kamińska[a,*], Tomasz Szymborski[a], Tomasz Jaroch[a], Adam Zmysłowski[b], Arkadiusz Szterk[b]

[a] Institute of Physical Chemistry, Polish Academy of Sciences, Kasprzaka 44/52, 01-224 Warsaw, Poland
[b] National Medicines Institute, Chełmska 30/34, 00-725 Warsaw, Poland

ARTICLE INFO

Keywords:
Porous silicone (PS)
Surface-enhanced Raman spectroscopy (SERS)
Blood
Urine
Cerebrospinal fluid

ABSTRACT

Surface-enhanced Raman spectroscopy (SERS) has been widely used in a variety of biomedical, analytical, forensic and environmental investigations due to its chemical specificity, label-free nature combined with high sensitivity. Here, we report a simple method for the fabrication of reproducible and reliable, well-defined, stable SERS substrates with uniform and giant Raman enhancement suitable for routine trace chemical analysis and detection of biological compounds in complex biological fluids. We prepared porous silicone (PS) surface by a galvanostatic anodic etch of crystalline silicon wafers. The electrochemical process generates a specific layer of PS: the thickness and porosity of a given layer is controlled by the current density, the duration of the etch cycle, and the composition of the etchant solution. These substrates presented high sensitivity to *p*-mercaptobenzoic acid (*p*-MBA) at a low concentration of 10^{-6} M and the enhancement factor of over 10^8 was achieved. Such high enhancement is attributed to semiconducting silicon-induced and stabilized hot spots. The uniform distribution of SERS–active 'hot-spots' on the Au/Si surface results in high reproducibility towards detecting *p*-MBA at 40 different, randomly selected positions on a single substrate (RSD = 6.7%) and on twenty different SERS substrates prepared under identical conditions (RSD = 8%). Designed substrates allow the ultrahigh sensitive and specific detection of human such biofluids as blood, urine and cerebrospinal fluid (CSF) in a reliable, label-free, and reproducible manner. The SERS spectra of these fluids are rich in patient-specific information and can be useful in many analytical and biomedical applications. We have shown that our developed SERS substrates allow the nanomolar detection of neopterin (bacterial infections' marker) in cerebrospinal fluid samples. In order to test the performance of our SERS method in term of low detection limit (LOD), the calibration curve i.e. plot of SERS intensity of the marker band at 695 cm^{-1} versus the concentration of neopterin in CSF was constructed and used to calculate the neopterin concentration in clinical samples. The level of neopterin was significantly higher in CSF samples infected by *Neisseria meningitidis*, (54 nmol/L), compared to normal (control) group, (4.3 nmol/L).

The high sensitivity, selectivity and stability of obtained SERS-active substrates combined with simple, low-cost, and easy method of producing offer a promising tool for SERS-based analysis in clinical trials.

1. Introduction

Surface-enhanced Raman scattering (SERS) is a powerful optical technique with high chemical specificity and sensitivity at trace concentration even down to single molecules [1–3]. The SERS effect is explained by the combination of an electromagnetic (EM) mechanism and a chemical mechanism related to charge transfer (CT) between a substrate and an adsorbed molecule [4]. The electromagnetic enhancement arises from the amplification of light by excitation of surface plasmon resonance (SPR) of the substrate. The chemical enhancement process involves the CT excitation between the frontier molecular orbitals of the adsorbate and the Fermi level of the metal substrate. This excitation may occur if the excitation wavelength is resonant with the metal-molecule charge transfer electronic states. There have been many experimental demonstrations confirming that of the two processes, the EM mechanism usually plays a larger role in SERS enhancement [5,6]. Theoretically, the electromagnetic enhancement can reach factors of 10^3–10^{11}, while the chemical enhancement factors up to 10^3 were calculated [7,8]. The EM enhancement is associated with the 'hot spots', which are spatially localized regions that exhibit extremely high

* Corresponding author.
E-mail address: akamin@ichf.edu.pl (A. Kamińska).

https://doi.org/10.1016/j.msec.2017.11.029
Received 8 June 2017; Received in revised form 23 August 2017; Accepted 22 November 2017
Available online 05 December 2017

field enhancement. Hot spots are created in the gap between two nanoparticles [9], but also near sharp edges, tips, and e.g., crossed nanowires [10]. The extremely large EM enhancement produced by these 'hot spots' combined with chemical enhancement give a huge total SERS cross-section, making single-molecule detection achievable. Additionally, the SERS technique offers nondestructive, reliable, multiplex and fast detection of analytes which leads to enormous applications of this technique. SERS is powerful in studying nucleic acids and proteins [11], therapeutic agents [12], drugs and trace materials [13], microorganisms [14], and cells [15]. The most notable recent advances in SERS include innovative applications of bimolecular sensors for clinical diagnosis of various diseases, such as breast [16] and prostate cancer [17].

An ideal SERS substrate should exhibits a uniform and high enhancement factor (EF), chemical stability, and the possibility to be produced cheaply and reproducibly. Although considerable development has been made towards improving and optimizing SERS substrates, the quantitative analysis of SERS and its practical applications in clinical trials have been hampered by the lack of effective SERS substrates which would satisfy all the requirements mentioned above. In general, a classical SERS substrate is based on Au and Ag, which have localized surface plasmon resonances in the visible and near infrared spectral regions. Silver nanostructures are most common and provide the largest enhancement but suffer from oxidation. Gold nanostructures are capable for use in numerous SERS applications, because of their large enhancement, biocompatibility, well-established functionalization chemistry, and air-stability and low reactivity [18].

Many techniques have been developed and used to produce highly uniform Ag and Au based SERS substrates optimized in size, shape, and composition. The production schemes include electrochemical methods [19] and colloidal suspension [20]. Recently, nanostructured surfaces for SERS analysis are tailored using given materials with the desired morphology (e.g. silicon, GaN) and then covered with gold or silver in order to convert these supports into SERS-active surfaces [21,22]. Such SERS substrates exhibit better nanostructure homogeneity with more reproducible SERS signals across a large area of surface in comparison to e.g., particle colloids. Generally, the electron-beam lithography [23], and nanoimprinting lithography [24] have been widely used to produce the materials of desired topology. Schmidt et al. [25,26] presented the method of Ag-capped silicon nanopilars SERS substrates fabrication using maskless lithography. Diebold [27] et al. reported the femtosecond laser-nanostructured silicon-based SERS substrates that exhibit uniform and high enhancement factor.

However, these approaches have very high fabrication cost of producing large substrate surface area and is dedicated mainly to laboratory applications. A broad variety of silicon-based nanostructures have been fabricated using wide ranges of plasma [28] and reactive ions [29,30] etching procedures. Still, these methods do not solve the current crucial issue in SERS substrate fabrication e.g., the better the reproducibility is across a substrate then the lower the enhancement of SERS signals can be usually recorded.

Nowadays, the tremendous efforts are made to perform sensitive, specific, and nondestructive SERS-based method for biological analysis, at both the molecular (e.g., immunomarkers, proteins, metabolites) and cellular levels (e.g., circulating tumor cells in blood). The blood plasma, cerebrospinal fluid and urine become very attractive as potential sources of many biomarkers therefore their spectroscopic analysis is crucial for development of biosensing applications of SERS technique.

In this paper we present a quick and easy method for producing the large areas of nanostructured substrate that satisfied both high, uniform enhancement factor and excellent reproducibility, since SERS hot spots are efficiently coupled and stabilized through interconnection to the semiconducting silicon substrates. A fabrication process has been developed using silicon ion etching method. A thin (30 nm) layer of gold sputtered on the silicon nanostructures provides activity to the obtained SERS platform.

The resultant SERS platforms show a very strong surface-enhancement factor (1×10^8), high stability (up to three months under ambient conditions), and high reproducibility, which could be used in the design of efficient SERS-active platforms for analytical applications. These Au/Si substrates exhibit good performance towards sensitive and reproducible SERS-based detection of complex human body fluids such as blood plasma, cerebrospinal fluid and urine.

2. Experimental section

2.1. Chemicals and materials

p-Mercaptobenzoic acid (*p*-MBA) and phosphate-buffered saline (PBS) packs (10 mM, pH = 7.2) from Sigma-Aldrich (Dorset, UK) were used without further purification. Water (resistivity over 18 MΩ), purified using a Milli-Q plus 185 system was used throughout the process. In our experiments we used human blood and urine samples from eight healthy volunteers available by courtesy of Regional Blood Center in Warsaw, Poland. Informed consent was obtained from all participants. All experiments were performed in compliance with the relevant laws and institutional guidelines. The protocol of study was approved by the Ethics and Bioethics Committee of Cardinal Stefan Wyszynski University in Warsaw. The artificial cerebrospinal sample fluid (aCSF) with physiologically identical concentrations of salts was purchased from Tocris Bioscience (Bristol, UK).

2.2. Instrumentation

2.2.1. Raman and SERS spectroscopy

Raman and SERS Spectroscopy measurements were carried out with a Renishaw inVia Raman system equipped with a 785 nm diode laser. The light from the laser was passed through a line filter and focused on a sample mounted on an X–Y–Z translation stage with a 20× microscope objective, NA = 0.25. The beam diameter was approximately 5 μm. The laser power at the sample was 5 mW or less. The microscope was equipped with 1200 grooves per mm grating, cutoff optical filters, and a 1024 × 256 pixel Peltier-cooled RenCam CCD detector, which allowed registering the Stokes part of Raman spectra with 5–6 cm^{-1} spectral resolution and 2 cm^{-1} wavenumber accuracy. The experiments were performed at ambient conditions using a back-scattering geometry.

2.2.2. SEM measurements

SEM measurements were performed under high vacuum using the FEI Nova NanoSEM 450 with an accelerating voltage from 2 kV to 10 kV.

2.2.3. AFM measurements

AFM measurements were carried out using the Atomic Force Microscopy (AFM) technique (Bruker, Dimension Icon with Scan Asyst). The Scanasyst-Air cantilever (silicon tip on nitride lever) was used for this investigation carried out in contact mode. The spring constant of the cantilevers used in the study was 0.4 N/m. Microscope was additionally protected from vibration by the use of an active table (Herzan TS-140^{+40} Low Power). The whole system was placed in a chamber (MBraun MB 200B) under dry argon atmosphere (O_2 and H_2O < 0.1 ppm).

2.3. Collecting of SERS spectra

For the recording of spectra, the SERS platform was placed into a chamber of 15 μl volume fabricated in polycarbonate. A 2 μl volume of the analyte solution was applied with a microliter syringe. The recording of the spectra was started immediately after placing this chamber under the microscope lens. During the period of at least 10 min, SERS spectra were repeatedly recorded, while at the same time,

the focus of the laser beam was readjusted. The time required for completing a single SERS spectrum was 4 s for *p*-MBA and 40 s for biological species (i.e. blood, urine, cerebrospinal fluid).

The obtained spectra were processed with an OPUS software (Bruker Optic GmbH 2012 version). The spectra were smoothed with Savitsky-Golay filter, the background was removed using baseline correction, and then the spectra were normalized using a so-called Min-Max normalization.

2.4. SERS substrate preparation

2.4.1. The ion etching procedure

Porous silicon samples were prepared by anodically etching p + + type, B-doped, ⟨100⟩ oriented silicon with resistivity 0.012 mΩ cm (Siltronix, Inc.) in a solution of 50% aqueous HF: organic solvent (3:1 by volume). The anodization was performed in a mixture of aqueous HF and the following solvents: mixture of pentanol:butanol:ethanol, proportion of each solvents were 1.0:0.25:0.25 (v/v), next separately propanol, isobutanol, acetonitrile, ethanol, tert-buthanol and butanol. The solutions were prepared from analytical-grade chemicals. The HF concentration was always the same in each solution. The anodization current was supplied by a Keithley 238 high-precision constant current source which is controlled by a computer to allow the formation of PS multilayers. Diagram electrochemical cells used to produce porous silicon by electrochemical etching was shown on Fig. 1. Typical etch parameters for a rugate structure involved a pseudosinusoidal current waveform oscillating between 11.5 and 19.2 mA·cm^{-2} with 50 repeats and a periodicity of 18 s. Films were removed from the substrate using a current pulse of 70 mA·cm^{-2} for 40 s. Example of potential development in HF/EtOH was shown on Fig. 2. To prevent the photogeneration of carriers, the anodization is performed in the dark. After formation the samples are rinsed with pure ethanol and dried with argon gas and immediately studied by Raman and SERS spectroscopy.

2.4.2. Procedure of gold sputtering

To sputter a layer of gold we used the PVD equipment from Leica, model EM MED020. The gold target was obtained from Mennica Metale Szlachetne, Warsaw, Poland. The size of the target was 54 mm in diameter, 0.5 mm thickness and gold purity was 5 N. The vacuum during the gold sputtering was on the level of 10^{-2} mbar. The sputtering current was 25 mA. After the deposition process the samples were placed into a sterile Petri dish. Six different thicknesses of gold (10, 30, 50, 100, 200 and 300 nm) were tested to find optimal conditions for SERS enhancement. The thickness of the layer was determined via AFM

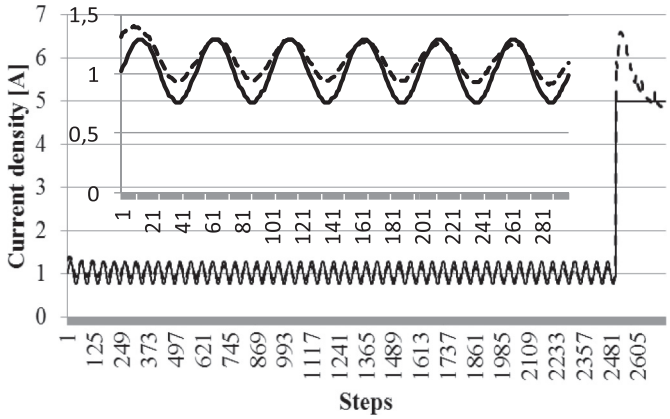

Fig. 2. Example of potential developments in HF/EtOH solutions. Black and intermittent curves show the current density controlled by the galvanostat and the potential measured by the reference electrode, respectively.

(see Section 2.2.3). Thin gold layers were deposited on silica by PVD method. After sputtering the polished side of Si we partially removed gold by stripping in many places to analyze the thickness of the edge of vaporized layers.

3. Results and discussion

3.1. Characterization of Au/Si surface

We prepared porous silicone (PS) surface by a galvanostatic anodic etch of crystalline silicon wafers. The electrochemical process generates a specific layer of PS: the thickness and porosity of a given layer is controlled by the current density, the duration of the etch cycle, and the composition of the etchant solution [5]. Structures approximating rugate filters [31] were prepared by applying a computer-generated pseudo-sinusoidal current waveform to the etch cell, following previously published procedures [32,33]. The resulting multilayers were removed from the substrate using a current pulse, and mechanically agitated or ultrasonicated to create particles [34]. HF solutions containing mainly ethanol are often used for the preparation of mesoporous silicon [35–37]. The role of alcohol in the electrolyte solution has been thought that it helps to reduce the surface tension on the pore wall resulting in the easy detachment of hydrogen gas that is formed during the hole (h) oxidation scheme as written in following reaction [38].

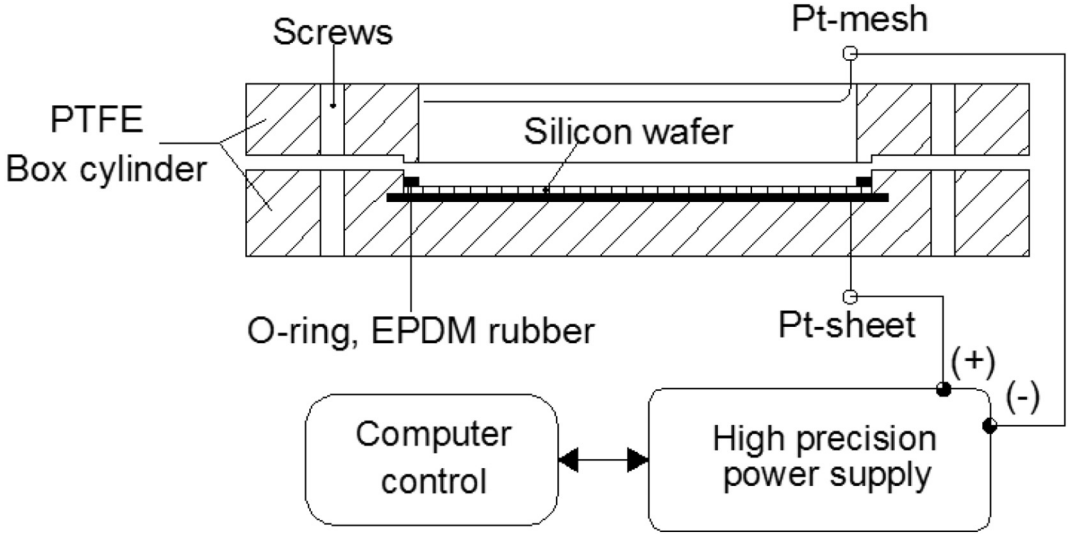

Fig. 1. Schemes of electrochemical cells used to produce porous silicon by electrochemical etching.

$$Si + 4HF_2^- + h^+ \rightarrow SiF_6^{2-} + 2HF + H_2 + e^-$$

By contrast, many groups have focused on the role of organic solvents in the formation of macroporous silicon [35,39–41] whose pore size is from several micrometers/nanometers to tens of micrometers. It has revealed that organic solvents have a strong impact on the formation of macroporous/mesoporous silicon [38,42,43]. In pore formation, it has reported that the surface of growing pore tips is covered with oxidized silicon, while the pore wall is terminated with Si—H bonds [32]. This means that bare (H-terminated) and oxidized silicon coexist on the pore wall surface of macroporous silicon. Understanding the affinity of organic solvents to macroporous silicon surface is thus highly complicated. On the other hand, the wall of porous silicon prepared in a high concentration of HF (~20 wt%) is not oxidized at all [44]. The analysis of the affinity between pore size and wall and an organic solvent must be much more straightforward than the case of macroporous/mesoporous silicon [43]. Moreover we do not have any information in terms of impact of various solvents in HF solution to create porous surface which can be used in SERS analysis. In our study we have developed seven procedures which were described in Table 1.

Fig. 3 shows the representative SEM images (for two different magnifications) of Au–coated PS surfaces (30 nm of gold) obtained by seven procedures. As can be seen the etching of the silicon creates porous, 3D structure. PS samples (I, II, III, V, VI, VII) revealed similar morphology in electron microscope, whereas substantial differences were observed for samples (IV) prepared at acetonitrile solution and sample (VIII) – control Si ⟨100⟩ surface. The characteristic length of the Au–coated PS samples (I, II, III, V, VI, VII) on the very top of the PS is in the range 50 nm to 150 nm, but the size of obtained nanostructures is significantly decreased to the range of 50–70 nm in the case of sample (VII). Sample (IV) does not possess porous structure, close examination of the sample (IV) and control sample (VIII) reveals that the sample (IV) was slightly etched only on the surface. SEM image at high magnification shows randomly placed several gold aggregates, with size 20–30 nm in diameter.

The influence of solvent in HF: solvent system (Table 1) on porous silicone formation during electrochemical eating can be explained by divergence in conductivity of used HF solution systems [35,39,42,45]. Water solutions of HF are characterised by a very high conductivity, around several hundred $mS{\cdot}cm^{-1}$ but HF solutions in alcohols or oxygen free solvent for instance acetonitrile, are characterised by much lower conductivity. Therefore the water solutions of HF are not used to obtain porous silicone surface in terms of speed of the process and lack of control of the process. There is some correlation between conductivity and HF:solvent system. Generally we observe decrease of conductivity of HF:solvent system with increase of carbon amount in used alcohol [42,45]. Moreover the conductivity is dramatically lower in oxygen free solvents. For instance the conductivity of HF:methanol solution (1:1.7 v/v) is around 54 $mS{\cdot}cm^{-1}$ but the same solution where methanol was replaced by tert-buthanol is around 37 $mS{\cdot}cm^{-1}$ and for acetonitrile it is below 5 $mS{\cdot}cm^{-1}$ [35,45]. Based on SEM analysis (Fig. 3) we observe that too low conductivity of solvent like acetonitrile used for silicone etching is not enough to obtain proper porous structure (Fig. 3, picture IV). However, too high conductivity of HF:solvent system leads to lower porosity. The highest porosity of silicon wafers was achieved when n-butanol and isobutanol were used in HF-solvent system.

3.2. SERS properties of Au/Si substrate

For evidence of SERS performance of prepared Au/Si substrates, molecule *p*-mercptobenzoic acid (*p*-MBA) was used to estimate their sensitivity and reproducibility. Due to the electronic off-resonant properties [46], *p*-MBA is adequate for multiwavelength studies. The recorded SERS signal intensities of *p*-MBA depend on the plasmonic characteristic of the SERS substrate. Moreover, the *p*-MBA molecules efficiently bind to the top gold layer of SERS-active surface through its thiol groups enables strong and stable SERS response.

In the first step, in order to examine the SERS sensitivity of the Au/Si substrates the enhancement factors (EF) for *p*-MBA we calculated. The obtained normal Raman and SERS spectra are depicted in Fig. S2. The Au/Si substrate was incubated in 9.0 mL of 1.0×10^{-6} M *p*-MBA solution in water for 60 min and then washed with deionized water. The Raman bands at 708, 796, 1072, 1176, 1474 and 1588 cm^{-1} are typical for *p*-MBA [47], and can be treated as a fingerprint of this molecule. Table S1 summarizes band assignments for the normal Raman spectrum of *p*-MBA and its SERS spectrum. The surface enhancement factor for *p*-MBA was calculated according to the following equation:

$$EF = \frac{I_{SERS} N_{NR}}{I_{NR} N_{SERS}} \quad (1)$$

where N_{SERS} and N_{NR} refer to the number of molecules adsorbed on the SERS probe within the laser spot area and the number of molecules probed by regular Raman spectroscopy, respectively. I_{SERS} and I_{NR} correspond to the SERS intensity of *p*-MBA on the modified surface and to the normal Raman scattering intensity of *p*-MBA in the bulk. I_{NR} and I_{SERS} were measured at 1072 cm^{-1}.

The crucial parameters for the quantitative analysis of the spectra are the laser spot area and the effective illuminated volume. The latter has been estimated using a formula recommended by Renishaw:

$$V = 3.21 \times \lambda^3 (f/D) \quad (2)$$

where *f* is the microscope objective focal length and D denotes the effective laser beam diameter at the objective back aperture. For our setup, $V = 2012 \approx 2 \times 10^3$ μm^3. The laser beam diameter, defined as twice the radius of a circle encompassing the area with 86% of the total power was about 5 μm; approximately the same values were obtained from the experimentally obtained laser spot image and from the theoretical formula ($4\lambda f / \pi D$). Assuming the volume in a shape of a cylinder with the diameter of 5 μm leads to the effective height of 100 μm. This value was confirmed by recording Raman spectra of Si while varying the distance from the focal plane. The SERS samples were prepared by dipping the substrate in 9.0 mL of 1.0×10^{-6} M solution of *p*-MBA. The number of molecules contained in the solution was 5.4×10^{15}

Table 1
Ion etching procedures used for preparation of PS.

Procedure ID	Solvent name	Solvent composition	HF concentration [mol l^{-3}]	Ion etching parameters
I	Pentanol:butanol:ethanol	1.0:0.25:0.25 (v/v)	18.7	Pseudo sinusoidal current waveform oscillating between 11.5 and 19.2 $mA{\cdot}cm^{-2}$ with 50 repeats and a periodicity of 18 s.
II	*n*-Propanol	100%		
III	Isobutanol	100%		
IV	Acetonitrile	100%		
V	Ethanol	100%		
VI	*tert*-Butanol	100%		
VII	*n*-Butanol	100%		
VIII	Control sample: Si wafer	–	–	–

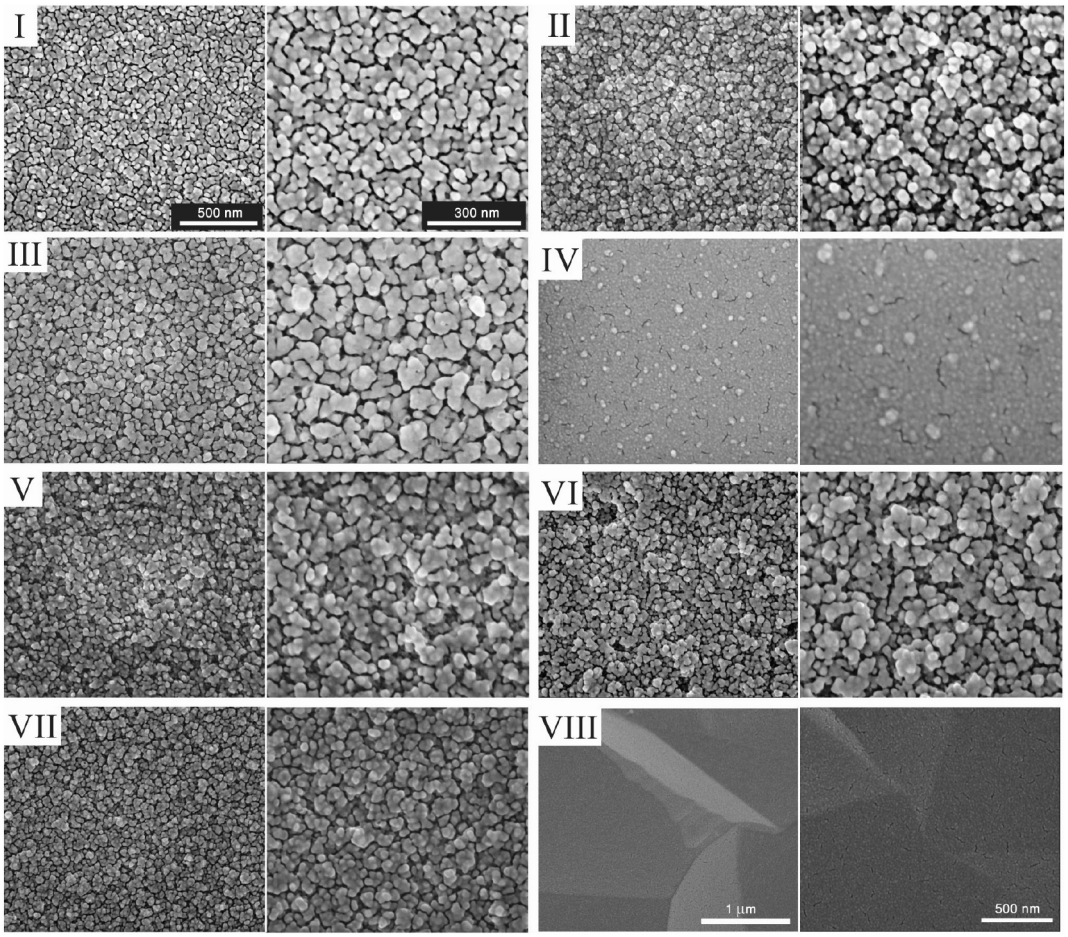

Fig. 3. SEM images of SERS-active platforms obtained by procedures described in Table 1. Etched silicon was covered with 30 nm layer of gold using PVD technique as described in Section 2.4.2.

(6.02×10^{23} molecules/mol $\times$ 9.0×10^{-3} L $\times$ 1.0×10^{-6} mol/L = 5.4×10^{15} molecules). The surface area irradiated by the laser beam (5 µm in diameter) was 19.6 µm^2 (3.14×2.5 µm^2 = 19.6 µm^2). The surface of our samples was 20 mm^2. Therefore, about 4.2×10^9 molecules were present in the laser beam spot. The normal Raman spectrum was observed for a cell filled with a pure *p*-MBA acid (154.19 g·mol^{-1}; density of 1.06 g·cm^{-3}). The effective illuminated volume for our setup is 2×10^3 µm^3. Under these conditions, $N_{NR} = 8.1 \times 10^{12}$ molecules were irradiated by the laser. From these data of the relative intensity and the number of molecules sampled from the regular Raman and SERS measurements, the enhancement factor was calculated to be about 4.2×10^7. The achieved level of enhancement makes this method of SERS platform fabrication a promising strategy for practical SERS applications.

SERS efficiency depends on surface morphology. We have tuned and optimized an etching ion processes by controlling the current density, the duration of the etch cycle, and the composition of the etchant solution (seven different procedures, see Table 1) to obtain a specific PS with appropriate nanostructures.

SERS spectra of *p*-MBA molecules adsorbed from 10^{-6} M aqueous solution onto these seven obtained surfaces (Fig. 3) have been recorded and presented in Fig. 4. Also, the enhancement factor for each surface (named from A to H) was calculated using Eq. (1) and presented in Table 2. The morphology of Au-coated PS (surface G) corresponds to the optimal size of nanostructures (50–70 nm) for the LSPR resonance [48], which results in the highest EF (Table 2). This huge value of the EF (10^8) is additionally amplified by the high efficient hot spots coupling and stabilization via interconnection to the semiconducting silicon [49].

Prior the SERS measurements the silicon nanostructures were coated with gold by PVD process to achieve the activity of the fabricated surfaces. The deposited film thickness determines the density and the size of gold particles formed on the surface [50]. Fig. 5 shows the dependence between the intensity of the 1072 cm^{-1} band and the thickness of the deposited gold film. The 10 nm gold layer was not sufficiently thick to obtain the appropriate SERS signal of the analyte (*p*-MBA and biofluids). The AFM images (see Fig. S1 in Supplementary materials) revel island-type covering of the surface of the silicon. Both, 30 nm and 50 nm layer of gold (Fig. S2) create an optimal size and distribution of gold particles for plasmon resonance effect for 735 nm excitation. The intensity of the marker bond at 1072 cm^{-1} significantly decreases with the increase of the gold thickness up to 1500 cps (counts per second) for 300 nm thick layer of Au. The correlation of the decrease of the intensity of the signal with increasing of the Au thickness layer is a result of change of the morphology of the surface of porous silicon: thicker layer of gold decrease porosity and roughness of the silicon, and lead to gold nanostructures at the size bigger than optimal for LSPR resonance [48] (see SEM images in Fig. 3).

To summarize: (i) the etching procedure VII (Table 1, Fig. 4) and (ii) 30 nm thickness of the Au metal film result the optimal morphology of silicon nanostructures for SERS applications. This optimized structure (G) has been used for further studies.

In the case of Si nanostructures covered with 30 nm of gold we observed the highest SERS enhancement and this thickness was applied for further experiments. Additionally, the SERS efficiency of this particular substrate has been tested at two another excitation wavelength e.g. 532 and 632.5 nm. Table S1 shows the intensities of representative SERS spectra of *p*-MBA adsorbed onto Au/Si substrates collected at the three excitation wavelengths 532, 632.8, and 725 nm, respectively. As can be seen, the marker bond at 1072 cm^{-1} shows an increase in SERS

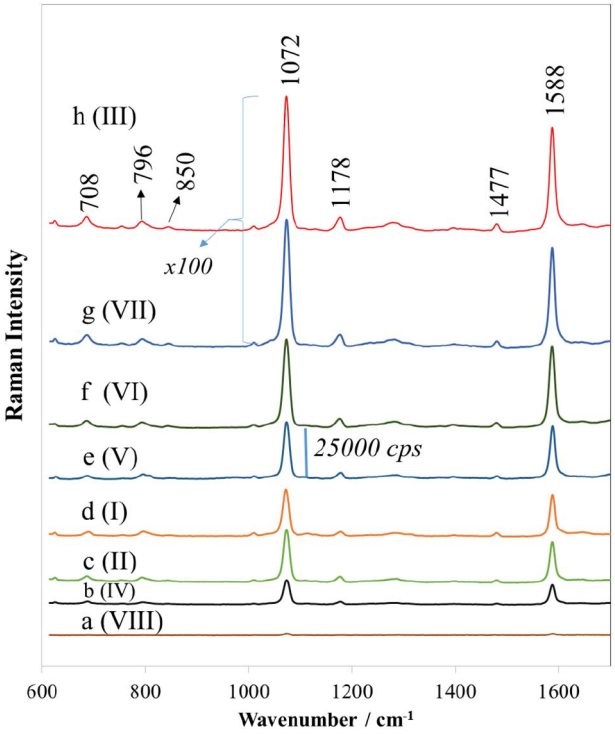

Fig. 4. SERS spectra of *p*-MBA recorded from seven different SERS substrates with varying morphology (according to procedures described in Table 1). Experimental conditions: 5 mW of 785 nm excitation, 2 × 2 s acquisition time. Each SERS spectrum was averaged from seven measurements in different places of SERS surface. The *p*-MBA spectra have been baseline corrected and shifted vertically for better visualization.

Table 2
The EF factors for SERS-active substrate obtained during seven different procedures of silicon etching (Table 1).

ID of etching procedure (Table 1) and corresponding SERS-active surface presented in Fig. 3		Enhancement factor (EF)
I	A	1.2×10^6
II	B	4.4×10^6
III	C	1.2×10^8
IV	D	1.7×10^4
V	E	3.5×10^6
VI	F	2.2×10^7
VII	**G**	$\mathbf{3.7 \times 10^8}$
VIII (ref.)	H	2.2×10^2

Bold data corresponds to the most sensitive SERS platform used in further experiments.

intensity ranging from 532 to 785 nm. As described in literature [51], the reflectance spectra of SERS substrates can typically reveal far-field electromagnetic enhancement mechanisms, whereast the near-field modes detect the intense long-wavelength resonance (700–800 nm) and explain these experimental results. Additionally, the use of this near-infrared excitation is the typical strategy for SERS analysis of biological samples as provides a compromise between signal level and background fluorescence [52,53] and therefore has been used for biological fluids analysis.

3.3. Stability and reproducibility of the SERS substrate

The reproducibility of recorded signals is one of the crucial parameter for bio-analytical and medical analysis. To verify the signal reproducibility the SERS intensity over a large area of the optimized SERS substrate (G), SERS spectra of *p*-MBA molecules (10^{-6} M) were collected. As can be seen in Fig. 6, the Au/Si substrate (G) exhibits very good SERS sensitivity and reproducibility. The Raman spectra of *p*-MBA

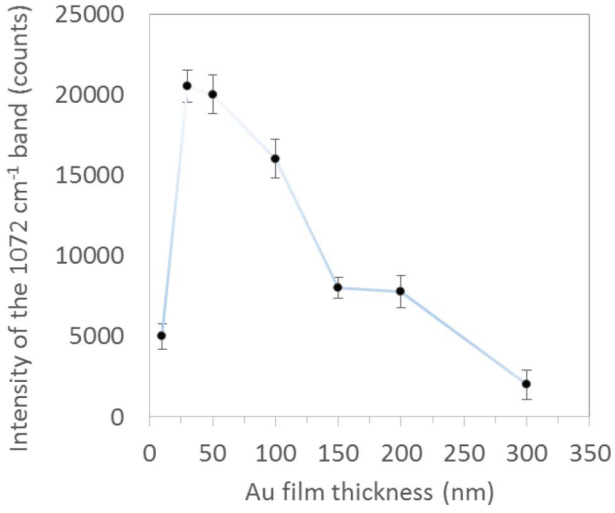

Fig. 5. The SERS intensity bands of the 1072 cm^{-1} with varying Au metal thickness (10 nm, 30 nm, 50 nm, 100 nm, 200 nm and 300 nm) for surface (G). The low intensity of the band 1072 cm^{-1} is the result of non-continuous cover of the surface of Si by Au layer (see Supporting materials for AFM results).

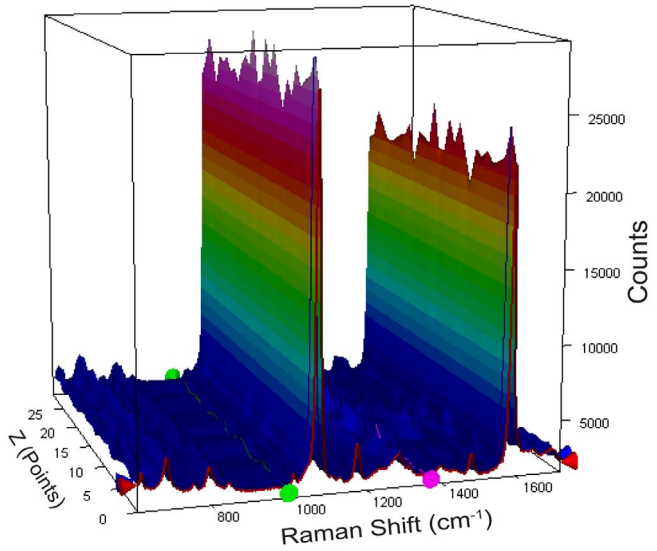

Fig. 6. The representative two-dimensional SERS spectra of *p*-MBA (10^{-6} M) recorded from 40 different spots on the SERS surface (G) using mapping mode. The spectra were collected over a distance of 1 mm with 10 μm steps (40 spectra are shown). Each point in the map was recorded using 5 mW of 785 nm excitation with 2 s integration times.

are enhanced strongly at each acquisition point. To get statistically meaningful results, the relative standard deviation (RSD) was calculated for the same band at 1072 cm^{-1} and equaled 6.7%. The reproducibility of the SERS signals recorded from different samples prepared using the same method was also tested. We collected 20 spectra from 20 different (separately fabricated) SERS platforms. The achieved RSD was 8%, which clearly indicates that the prepared SERS substrate can be considered as a highly reproducible SERS platform. The obtained RSD value for our substrates is comparable to the RSD value of a commercial substrate Klarite (RSD = 14%). So far, the quantitative analysis of SERS and its practical applications in clinical trials have been hampered by irreproducible production of SERS substrate e.g. variation in surface roughness and SERS signals.

The stability of a SERS substrate determines the range of its practical applications in chemical and biological analysis. The crucial parameters are the stability against oxidation for an extended period of time. Fig. 7 illustrates the SERS spectra of *p*-MBA recorded on a freshly

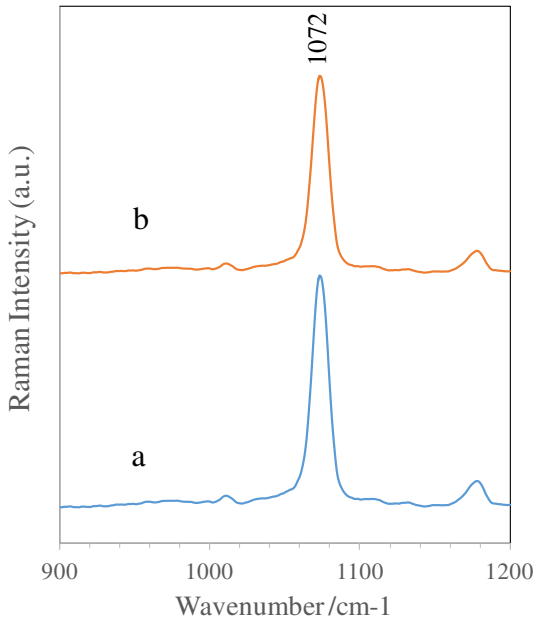

Fig. 7. SERS spectra of *p*-MBA recorded on (a) freshly prepared Au/Si surface (G) and (b) on the Au/Si surface (G) stored for three months under ambient conditions. Experimental conditions: 5 mW of 785 nm excitation, 2 × 2 s acquisition time. Each SERS spectrum was averaged from 15 measurements at different places across the SERS surface.

prepared Au/Si surface (Fig. 7a) and on a surface exposed to air for six weeks. Considering the 1072 cm^{-1} band as a reference, the intensity of *p*-MBA was reduced approximately by only 3% after three months of storing the surface under atmospheric conditions (Fig. 7b). Such high stability and reproducibility enables the quantitative SERS studies of numerous biomolecules and improves the SERS potential in real applications.

To summarize, all of these results show an excellent sensitivity, reproducibility, and stability of obtained SERS substrate (G) and are highly promising for the detection biological species.

3.4. Label-free SERS analysis of human biofluids

In clinical practice, the human biofluids such as blood, plasma, urine, saliva, and cerebrospinal fluids are the main objectives to obtain diagnostic information. The biofluids possess a vest amount of patient–specific information that can be used to describe the local pathologies as well as systemic diseases, detection and monitoring of drug compliance and response, monitoring baseline on specific biomarkers [54]. The label-free SERS analysis of biofluids is essential for the development of novel, rapid, inexpensive, and in-point of care detection and monitoring of various biological fluids. The results of this study demonstrate the potential of our developed SERS-active surface (G) to examine such complex chemical mixture as the blood, urine and cerebrospinal fluids. Human blood (and its liquid component plasma or serum) is routinely collected as clinical specimens from patients.

Before SERS measurements, the normal Rama spectra of all analyzed samples: the whole blood plasma, urine, and cerebrospinal fluid are recorded to allow a comparison with the corresponding, subsequently described 785 nm excited SERS spectra of these fluids. Fig. S3 presents the representative Raman spectra of investigated human biofluids. The observed Raman vibrational frequencies of liquid whole human blood (Fig. S3a), and their corresponding vibrational assignments are discussed in Supplementary materials and summarized in Table 3.

Fig. 8 shows the SERS spectrum of whole human blood plasma placed onto optimized SERS-active surface (G).

The SERS spectrum display many bands typical for porphyrin (796, 863, 1215, and 1446, 1562 and 1609 cm^{-1}), as well as signals assigned to globin vibrations (638, 716, 904, 1002, 1027, 1257, and 1342 cm^{-1}), and some others, which may include contribution from proteins and lipids (956, 1104, 1128, 1257, 1562 cm^{-1}). The observed SERS vibrational frequencies of liquid whole human blood (Fig. 8a) and their corresponding vibrational assignments are summarized in Table 3.

Urine is an human biofluids produced during the elimination of numerous bioproducts of the metabolism from the bloodstream [59]. The most important component of urine is water and urea. Beside these, urine contains small amount of creatinine, uric acid, and albumin [60]. To explore the SERS potential of our developed substrate the human urine samples were investigated. Fig. 8b presents the representative SERS spectrum from 40 randomly selected spots of SERS-active surface C. The most intensive band at 1002 cm^{-1} corresponds to the N—C—N stretching vibrations of the urea molecule, confirming that this band can be directly used for urea analysis. Another bands at 623 cm^{-1} (O═C—N deformation), 809 cm^{-1} (creatinine), 1134 cm^{-1} (C—N stretching), 1376 cm^{-1} (tryptophan vibration), and 1589 cm^{-1} (ring stretching) [61] can be also identified as human urine. The vibrational frequencies of the bands observed in recorded SERS spectrum of urine and the bands assignments are listed in Table 4.

As can be seen from Fig. 8c the good quality of SERS spectra were also obtained for cerebrospinal fluid (CSF) samples deposited on a sample D. CSF often called as liquor, is clinically used as a diagnostic fluid for diseases such as meningitis [62,63], myelitis and multiple sclerosis [64]. CSF of healthy patient contains no erythrocytes and up to five leukocytes per microliter [65]. As can be seen in Fig. 1a the intensive bands at 729, 1134, 1329, 1612 cm^{-1} were assigned to vibrations of the nucleic bases of DNA and lipids [66]. The features at 1470, 1250, and 1006 cm^{-1} are associated to the CH_2 deformation, the amide III, the symmetric ring breathing bands of phenylalanine and protein, and C—C stretching, respectively [67]. Aromatic amino acid residues, phenylalanine, tyrosine, and tryptophan were expected to have bands at 1006, 625, 659, 866, and 1243 cm^{-1}.

3.5. Analytical performance of Au/Si substrate

In order to validate the performance of our SERS surface in terms of analytical sensitivity and low detection limit (LOD) the concentration dependence of neopterin (bacterial infections' marker) in cerebrospinal fluid (CSF) has been examined. Neopterin (NP), a pyrazonopyrimidine compound is synthesized from guanosine triphosphate by human monocytes and macrophages after stimulation by interferon gamma (IFN-γ) derived from antigen-activated T lymphocytes [68]. The high level of neopterin is associated with viral (hepatitis A, B, and C, Cytomegalo, measles, rubella, influenza) and bacterial infections [69], cardiovascular disease [70], insulin resistance [71], and some tumors [72]. Bacterial meningitis might be associated with both elevated serum and cerebrospinal fluid (CSF) neopterin levels compared to controls. Additionally, neopterin is a small molecule which is biologically and chemically stable in body fluids, gives strong SERS signals and therefore can be applied for label–free measurements in the laboratory using the Raman technique [73]. In our studies the normal CSF (from healthy patent) and the CSF samples infected by *Neisseria meningitidis* have been analyzed. The calibration curve i.e. plot of SERS intensity of the marker band of neopterin at 695 cm^{-1} versus the concentration of neopterin in CSF (artificially added) was constructed and used to calculate the neopterin concentration in clinical samples (Fig. S4). The samples of neopterin in CSF with different concentrations, reflecting clinically relevant neopterin titers, (0–100 nmol/L) were prepared.

In the linear region the calibration curve was fitted as $y = 0.0899x$ and the correlation coefficient (R^2) was 0.997. For the linear calibration curve, it was assumed that the SERS intensity at 695 cm^{-1} (y) is linearly related to the concentration of neopterin (x). The low detection limit (LOD) was estimated using the signal-to-noise method [74]. The calculated level of neopterin was significantly higher in CSF samples

Table 3
Observed Raman and SERS vibrational bands of whole human blood (liquid droplet) at 785 nm and their assignments [55–58]. Vibrations: n – valence, d – deformation, g – deformation (out of plane).

SERS ν (cm^{-1})	Raman ν (cm^{-1})	Vibrational mode	Assignment
638	641	C–S stretch	Globin and cellular components (cysteine)
716	738	$d(COO^-)$	Globin and cellular components (amino-acids)
796		n(pyr breathe), n_6	Porphyrin
863		$g(C_mH)$	Porphyrin
904		C–C stretch	Globin and cellular components (glutamic acid, isoleucine, threonine, lysine)
956		C–C stretch	Globin and cellular components (proteins)
1002	1003	Indole asymmetric ring breathe	Globin and cellular components (phenylalanine)
1027	1025	in plane ring CH deform	Globin and globin and cellular components (phenylalanine)
1104		C–N, C–C stretch	Globin and cellular components (proteins, lipids)
1127	1128	C–N, C–C stretch	Globin and cellular components (proteins)
1215	1220	$d(C_mH)$, n_{13} or n_{42}	Porphyrin
1257	1252	CH_2 wagging $d(CH_2/CH_3)_6$	Globin (glutamic acid) and cellular components (proteins, lipids: amide iii)
1286	1284	$g(C_mH)$, n_{21}	Porphyrin
1326		CH_2 wagging	Globin and cellular components (phenylalanine, glutamic acid, serine, methionine, histidine)
1342	1342	CH_2 scissoring CH_3 deformation	Globin and cellular components - glutamic acid, aspartic acid, asparagine, glutamine; - alanine, leucine, valine, isoleucine
1446	1446	$d(CH_2/CH_3)$	Globin and porphyrin
1488		CH and ring	Tryptophan
1562	1569		Porphyrin (skeletal mode) and cellular components
1609			Porphyrin

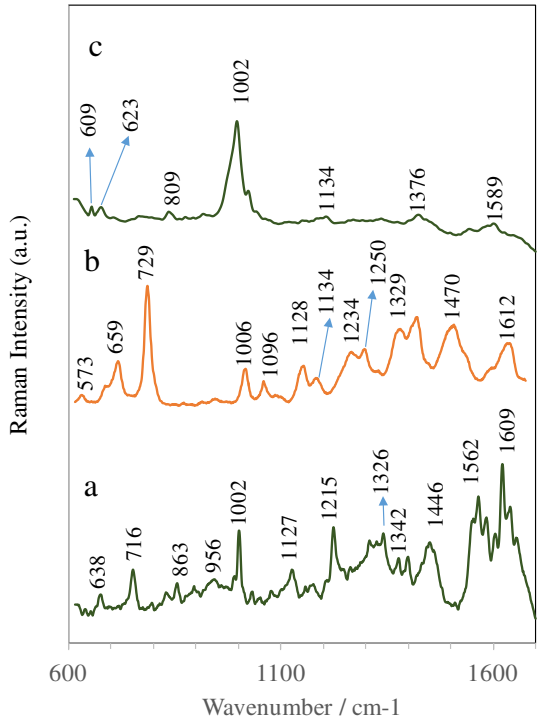

Fig. 8. Average SERS spectra of (a) whole human blood, (b) cerebrospinal fluids and (c) urine obtained onto optimized SERS-active Au/Si surface (G). Mean spectra were averaged over 30 spectra from different spots. Experimental conditions: 5 mW of 785 nm excitation, 4 × 10 s acquisition time. The SERS spectra have been baseline corrected and shifted vertically for better visualization.

infected by *Neisseria meningitidis*, (54 nmol/L), compared to normal (control) group, (4.3 nmol/L). The deeper SERS analysis of normal ad infected CSF samples is presented in the Supplementary materials.

4. Conclusions

The present study demonstrates the new approach in the development of silicon-based SERS-active substrate. The influence of etching solutions and Au metal thickness on SERS efficiency was investigated and the optimal fabrication process parameters were proved. In result,

Table 4
Observed vibrational bands of urine (liquid droplet) at 785 nm and their assignments [61]. Vibrations: n – valence, d – deformation, g – deformation (out of plane).

SERS ν (cm^{-1})	Vibrational mode	Assignment
609	Anti-symmetric stretching vibration of PO_3^{4-}	Cholesterol ester/nucleic acids
623	O=C–N deformation	Uric acid
809	C–C stretching vibration	Albumin
889	C–O–H twist vibration	D-Galactosamine
959	symmetric stretching vibration of PO_3^{4-}	Hydroxyproline
1006	C–N stretching vibration	Urea
1134	H–C–N twist and rock	Phenylalanine
1376	Ring breathing modes/C–H twist vibration	Tryptophan
1589	Ring stretches	Phenylalanine

the easy, simple (two steps), and low-cost procedure for reproducible large scale fabrication of new SERS substrates was established.

Our experimental results indicate that this SERS-active substrate with its strong surface-enhancement factor, high stability and reproducibility can be used for label–free SERS detection in both, biological and non-biological samples. For *p*-mercaptobenzoic acid the enhancement factor (EF) of the Raman signal on a Si/Au surface (G) was estimated as high as 10^8. The SERS measurement reflects the excellent reproducibly of these substrates, both between platforms and across the single platform.

Moreover, our developed SERS substrates offer a rapid, sensitive, high-throughput, suitable for point-of-care analysis of human biofluids such as blood, urine, and cerebrospinal fluid. In clinical practice, these fluids provide the main medical information, that can be utilized for diagnostic purposes. As an example, our results illustrate the potential of Au/Si SERS substrate for detection of neopterin (immune marker) in cerebrospinal fluids samples.

Acknowledgements

Agnieszka Kamińska thanks for the financial support from National Science Centre under grant UMO-2015/17/B/ST4/04128. Arkadiusz Szterk and Adam Zmysłowski thanks for the financial support from Ministry of Science and Higher Education Republic of Poland under statute grand number NIL-DS 1.34. We would also like to thank prof.

Robert Nowakowski from the Institute of Physical Chemistry of the Polish Academy of Sciences for sharing the AFM microscope for research and discussion of experimental results. We also thank prof. A. Skoczyńska from National Medicines Institute for clinical CSF samples.

Appendix A. Supplementary data

Supplementary data to this article can be found online at https://doi.org/10.1016/j.msec.2017.11.029.

References

[1] S.M. Nie, S.R. Emery, Probing single molecules and single nanoparticles by surface-enhanced Raman scattering, Science 275 (1997) 1102–1106.
[2] Y.Q. Wang, B. Yan, L.X. Chen, S.E.R.S. Tags, Novel optical nanoprobes for bioanalysis, Chem. Rev. 113 (2013) 1391–1428.
[3] A. Hakonen, T. Rindzevicius, M.S. Schmidt, P.O. Andersson, L. Juhlin, M. Svedendahl, A. Boisen, M. Kall, Detection of nerve gases using surface-enhanced Raman scattering substrates with high droplet adhesion, Nano 8 (2016) 1305–1308.
[4] A. Campion, P. Kambhampati, Surface-enhanced Raman scattering, Chem. Soc. Rev. 27 (1998) 241–250.
[5] L.T. Canham, INSPEC, Properties of Porous Silicon, INSPEC, 1997.
[6] L. Chen, J. Choo, Recent advances in surface-enhanced Raman scattering detection technology for microfluidic chips, Electrophoresis 29 (2008) 1815–1828.
[7] P.L. Stiles, J.A. Dieringer, N.C. Shah, R.P. Van Duyne, Surface-enhanced Raman spectroscopy, Annu Rev Anal Chem (Palo Alto, Calif) 1 (2008) 601–626.
[8] J.P. Camden, J.A. Dieringer, Y. Wang, D.J. Masiello, L.D. Marks, G.C. Schatz, R.P. Van Duyne, Probing the structure of single-molecule surface-enhanced Raman scattering hot spots, J. Am. Chem. Soc. 130 (2008) 12616–12617.
[9] M. Li, S.K. Cushing, J. Zhang, J. Lankford, Z.P. Aguilar, D. Ma, N. Wu, Shape-dependent surface-enhanced Raman scattering in gold-Raman probe-silica sandwiched nanoparticles for biocompatible applications, Nanotechnology 23 (2012) 115501.
[10] G. Braun, I. Pavel, A.R. Morrill, D.S. Seferos, G.C. Bazan, N.O. Reich, M. Moskovits, Chemically patterned microspheres for controlled nanoparticle assembly in the construction of SERS hot spots, J. Am. Chem. Soc. 129 (2007) 7760–7761.
[11] K. Kneipp, H. Kneipp, V.B. Kartha, R. Manoharan, G. Deinum, I. Itzkan, R.R. Dasari, M.S. Feld, Detection and identification of a single DNA base molecule using surface-enhanced Raman scattering (SERS), Phys. Rev. E 57 (1998) R6281–R6284.
[12] R.J. Stokes, E. McBride, C.G. Wilson, J.M. Girkin, W.E. Smith, D. Graham, Surface-enhanced Raman scattering spectroscopy as a sensitive and selective technique for the detection of folic acid in water and human serum, Appl. Spectrosc. 62 (2008) 371–376.
[13] K. Faulds, W.E. Smith, D. Graham, R.J. Lacey, Assessment of silver and gold substrates for the detection of amphetamine sulfate by surface enhanced Raman scattering (SERS), Analyst 127 (2002) 282–286.
[14] A. Sivanesan, E. Witkowska, W. Adamkiewicz, L. Dziewit, A. Kaminska, J. Waluk, Nanostructured silver-gold bimetallic SERS substrates for selective identification of bacteria in human blood, Analyst 139 (2014) 1037–1043.
[15] T.A. Alexander, D.M. Le, Characterization of a commercialized SERS-active substrate and its application to the identification of intact Bacillus endospores, Appl. Opt. 46 (2007) 3878–3890.
[16] T. Vo-Dinh, L.R. Allain, D.L. Stokes, Cancer gene detection using surface-enhanced Raman scattering (SERS), J. Raman Spectrosc. 33 (2002) 511–516.
[17] H.W. Tang, X.B. Yang, J. Kirkham, D.A. Smith, Probing intrinsic and extrinsic components in single osteosarcoma cells by near-infrared surface-enhanced Raman scattering, Anal. Chem. 79 (2007) 3646–3653.
[18] G.A. Baker, D.S. Moore, Progress in plasmonic engineering of surface-enhanced Raman-scattering substrates toward ultra-trace analysis, Anal. Bioanal. Chem. 382 (2005) 1751–1770.
[19] H.H. Wang, C.Y. Liu, S.B. Wu, N.W. Liu, C.Y. Peng, T.H. Chan, C.F. Hsu, J.K. Wang, Y.L. Wang, Highly Raman-enhancing substrates based on silver nanoparticle arrays with tunable sub-10 nm gaps, Adv. Mater. 18 (2006) (491-+).
[20] K. Faulds, W.E. Smith, D. Graham, Evaluation of surface-enhanced resonance Raman scattering for quantitative DNA analysis, Anal. Chem. 76 (2004) 412–417.
[21] X.Y. Zhang, C.R. Yonzon, R.P. Van Duyne, Nanosphere lithography fabricated plasmonic materials and their applications, J. Mater. Res. 21 (2006) 1083–1092.
[22] A. Kaminska, I. Dziecielewski, J.L. Weyher, J. Waluk, S. Gawinkowski, V. Sashuk, M. Fialkowski, M. Sawicka, T. Suski, S. Porowski, R. Holyst, Highly reproducible, stable and multiply regenerated surface-enhanced Raman scattering substrate for biomedical applications, J. Mater. Chem. 21 (2011) 8662–8669.
[23] D.P. Fromm, A. Sundaramurthy, A. Kinkhabwala, P.J. Schuck, G.S. Kino, W.E. Moerner, Exploring the chemical enhancement for surface-enhanced Raman scattering with Au bowtie nanoantennas, J. Chem. Phys. 124 (2006) 61101.
[24] R. Alvarez-Puebla, B. Cui, J.-P. Bravo-Vasquez, T. Veres, H. Fenniri, Nanoimprinted SERS-active substrates with tunable surface plasmon resonances, J. Phys. Chem. C 111 (2007) 6720–6723.
[25] M.S. Schmidt, J. Hubner, A. Boisen, Large area fabrication of leaning silicon nanopillars for surface enhanced Raman spectroscopy, Adv. Mater. 24 (2012) OP11–OP18.
[26] J. Yang, M. Palla, F.G. Bosco, T. Rindzevicius, T.S. Alstrom, M.S. Schmidt, A. Boisen, J.Y. Ju, Q. Lin, Surface-enhanced Raman spectroscopy based quantitative bioassay on aptamer-functionalized nanopillars using large-area Raman mapping, ACS Nano 7 (2013) 5350–5359.
[27] E.D. Diebold, N.H. Mack, S.K. Doorn, E. Mazur, Femtosecond laser-nanostructured substrates for surface-enhanced Raman scattering, Langmuir 25 (2009) 1790–1794.
[28] Y.S. Hu, J. Jeon, T.J. Seok, S. Lee, J.H. Hafner, R.A. Drezek, H. Choo, Enhanced Raman scattering from nanoparticle-decorated nanocone substrates: a practical approach to harness in-plane excitation, ACS Nano 4 (2010) 5721–5730.
[29] M.S. Schmidt, A. Boisen, J. Hübner, Towards easily reproducible nano-structured SERS substrates, IEEE (2009) 1763–1767.
[30] J. Tang, F.S. Ou, H.P. Kuo, M. Hu, W.F. Stickle, Z.Y. Li, R.S. Williams, Silver-coated Si nanograss as highly sensitive surface-enhanced Raman spectroscopy substrates, Appl. Phys. A Mater. Sci. Process. 96 (2009) 793–797.
[31] M.G. Berger, R. ArensFischer, M. Thonissen, M. Kruger, S. Billat, H. Luth, S. Hilbrich, W. Theiss, P. Grosse, Dielectric filters made of PS: advanced performance by oxidation and new layer structures, Thin Solid Films 297 (1997) 237–240.
[32] V. Lehmann, R. Stengl, H. Reisinger, R. Detemple, W. Theiss, Optical shortpass filters based on macroporous silicon, Appl. Phys. Lett. 78 (2001) 589–591.
[33] S. Zangooie, M. Schubert, C. Trimble, D.W. Thompson, J.A. Woollam, Infrared ellipsometry characterization of porous silicon Bragg reflectors, Appl. Opt. 40 (2001) 906–912.
[34] J.L. Heinrich, C.L. Curtis, G.M. Credo, M.J. Sailor, K.L. Kavanagh, Luminescent colloidal silicon suspensions from porous silicon, Science 255 (1992) 66–68.
[35] M. Christophersen, J. Carstensen, K. Voigt, H. Foll, Organic and aqueous electrolytes used for etching macro- and mesoporous silicon, Phys. Status Solidi A 197 (2003) 34–38.
[36] P. Kumar, T. Hofmann, K. Knorr, P. Huber, P. Scheib, P. Lemmens, Tuning the pore wall morphology of mesoporous silicon from branchy to smooth, tubular by chemical treatment, J. Appl. Phys. 103 (2008) 6.
[37] V. Lehmann, R. Stengl, A. Luigart, On the morphology and the electrochemical formation mechanism of mesoporous silicon, Mater. Sci. Eng. B 69 (2000) 11–22.
[38] S.N. Sharma, R. Sharma, S.T. Lakshmikumar, Role of an electrolyte and substrate on the stability of porous silicon, Phys. E. 28 (2005) 264–272.
[39] C. Levy-Clement, S. Lust, M. Mamor, J. Rappich, T. Dittrich, Investigation of p-type macroporous silicon formation, Phys. Status Solidi A 202 (2005) 1390–1395.
[40] P. Bettotti, L. Dal Negro, Z. Gaburro, L. Pavesi, A. Lui, M. Galli, M. Patrini, F. Marabelli, P-type macroporous silicon for two-dimensional photonic crystals, J. Appl. Phys. 92 (2002) 6966–6972.
[41] H. Foll, M. Leisner, A. Cojocaru, J. Carstensen, Macroporous semiconductors, Materials 3 (2010) 3006–3076.
[42] T. Urata, K. Fukami, T. Sakka, Y.H. Ogata, Pore formation in p-type silicon in solutions containing different types of alcohol, Nanoscale Res. Lett. 7 (2012) 5.
[43] T. Urata, K. Fukami, T. Sakka, Y.H. Ogata, Morphological development from uniform microporous structure to macropore-like structure, ECS Trans. 50 (2013) 61–74.
[44] Y. Ogata, H. Niki, T. Sakka, M. Iwasaki, Hydrogen in porous silicon: vibrational analysis of SiHx species, J. Electrochem. Soc. 142 (1995) 195–201.
[45] T. Urata, K. Fukami, N. Takeda, T. Sakka, Y.H. Ogata, Influence of solvents in HF solutions on anodic formation of mesoporous silicon, revealed by the characterization of mesoporous silicon Rugate filters, ECS J. Solid State Sci. Technol. 5 (2016) P250–P255.
[46] E. Campaigne, W.W. Meyer, Preparation and absorption spectra of p-mercaptocinnamic and p-mercaptobenzoic acids and derivatives, J. Organomet. Chem. 27 (1962) (2835-&).
[47] A. Michota, J. Bukowska, Surface-enhanced Raman scattering (SERS) of 4-mercaptobenzoic acid on silver and gold substrates, J. Raman Spectrosc. 34 (2003) 21–25.
[48] S.N. Terekhov, S.M. Kachan, A.Y. Panarin, P. Mojzes, Surface-enhanced Raman scattering on silvered porous alumina templates: role of multipolar surface plasmon resonant modes, Phys. Chem. Chem. Phys. 17 (2015) 31780–31789.
[49] Y. He, S. Su, T. Xu, Y. Zhong, J.A. Zapien, J. Li, C. Fan, S.-T. Lee, Silicon nanowires-based highly-efficient SERS-active platform for ultrasensitive DNA detection, Nano Today 6 (2011) 122–130.
[50] Y. Fang, N.H. Seong, D.D. Dlott, Measurement of the distribution of site enhancements in surface-enhanced Raman scattering, Science 321 (2008) 388–392.
[51] C. Novara, S. Dalla Marta, A. Virga, A. Lamberti, A. Angelini, A. Chiado, P. Rivolo, F. Geobaldo, V. Sergo, A. Bonifacio, F. Giorgis, SERS-active ag nanoparticles on porous silicon and PDMS substrates: a comparative study of uniformity and Raman efficiency, J. Phys. Chem. C 120 (2016) 16946–16953.
[52] W. Hill, V. Petrou, Caries detection by diode laser Raman spectroscopy, Appl. Spectrosc. 54 (2000) 795–799.
[53] M.V. Schulmerich, J.H. Cole, K.A. Dooley, M.D. Morris, J.M. Kreider, S.A. Goldstein, S. Srinivasan, B.W. Pogue, Noninvasive Raman tomographic imaging of canine bone tissue, J. Biomed. Opt. 13 (2008) 3.
[54] A. Subaihi, L. Almanqur, H. Muhamadali, N. AlMasoud, D.I. Ellis, D.K. Trivedi, K.A. Hollywood, Y. Xu, R. Goodacre, Rapid, accurate, and quantitative detection of propranolol in multiple human biofluids via surface-enhanced Raman scattering, Anal. Chem. 88 (2016) 10884–10892.
[55] S. Stewart, P.M. Fredericks, Surface-enhanced Raman spectroscopy of amino acids adsorbed on an electrochemically prepared silver surface, Spectrochim. Acta A Mol. Biomol. Spectrosc. 55 (1999) 1641–1660.
[56] N.A. Brazhe, S. Abdali, A.R. Brazhe, O.G. Luneva, N.Y. Bryzgalova, E.Y. Parshina, O.V. Sosnovtseva, G.V. Maksimov, New insight into erythrocyte through in vivo surface-enhanced Raman spectroscopy, Biophys. J. 97 (2009) 3206–3214.
[57] J.L. Lippert, L.E. Gorczyca, G. Meiklejohn, A laser Raman spectroscopic investigation of phospholipid and protein configurations in hemoglobin-free erythrocyte

ghosts, Biochim. Biophys. Acta 382 (1975) 51–57.
[58] D.F. Wallach, S.P. Verma, Raman and resonance-Raman scattering by erythrocyte ghosts, Biochim. Biophys. Acta 382 (1975) 542–551.
[59] A. Bonifacio, S. Cervo, V. Sergo, Label-free surface-enhanced Raman spectroscopy of biofluids: fundamental aspects and diagnostic applications, Anal. Bioanal. Chem. 407 (2015) 8265–8277.
[60] W.R. Premasiri, R.H. Clarke, M.E. Womble, Urine analysis by laser Raman spectroscopy, Lasers Surg. Med. 28 (2001) 330–334.
[61] G. Trachta, B. Schwarze, B. Sägmüller, G. Brehm, S. Schneider, Combination of high-performance liquid chromatography and SERS detection applied to the analysis of drugs in human blood and urine, J. Mol. Struct. 693 (2004) 175–185.
[62] A. Kaminska, E. Witkowska, A. Kowalska, A. Skoczynska, P. Ronkiewicz, T. Szymborski, J. Waluk, Rapid detection and identification of bacterial meningitis pathogens in ex vivo clinical samples by SERS method and principal component analysis, Anal. Methods 8 (2016) 4521–4529.
[63] A. Kaminska, E. Witkowska, A. Kowalska, A. Skoczynska, I. Gawryszewska, E. Guziewicz, D. Snigurenko, J. Waluk, Highly efficient SERS-based detection of cerebrospinal fluid neopterin as a diagnostic marker of bacterial infection, Anal. Bioanal. Chem. 408 (2016) 4319–4327.
[64] https://www.bioanalysis-zone.com/2016/02/08/chapter-6-personalized-proteomics-of-human-biofluids-for-clinical-applications/.
[65] M. Harz, M. Kiehntopf, S. Stockel, P. Rosch, T. Deufel, J. Popp, Analysis of single blood cells for CSF diagnostics via a combination of fluorescence staining and micro-Raman spectroscopy, Analyst 133 (2008) 1416–1423.
[66] J.W. Chan, D.S. Taylor, S.M. Lane, T. Zwerdling, J. Tuscano, T. Huser, Nondestructive identification of individual leukemia cells by laser trapping Raman spectroscopy, Anal. Chem. 80 (2008) 2180–2187.
[67] Z. Movasaghi, S. Rehman, I.U. Rehman, Raman spectroscopy of biological tissues, Appl. Spectrosc. Rev. 42 (2007) 493–541.
[68] C. Huber, J.R. Batchelor, D. Fuchs, A. Hausen, A. Lang, D. Niederwieser, G. Reibnegger, P. Swetly, J. Troppmair, H. Wachter, Immune-response associated production of neopterin - release from macrophages primarily under control of interferon-gamma, J. Exp. Med. 160 (1984) 310–316.
[69] D. Fuchs, A. Hausen, M. Kofler, H. Kosanowski, G. Reibnegger, H. Wachter, Neopterin as an index of immune-response in patients with tuberculosis, Lung 162 (1984) 337–346.
[70] X. Garcia-Moll, D. Cole, E. Zouridakis, J.C. Kaski, Increased serum neopterin: a marker of coronary artery disease activity in women, Heart 83 (2000) 346–350.
[71] M. Ledochowski, C. Murr, B. Widner, D. Fuchs, Association between insulin resistance, body mass and neopterin concentrations, Clin. Chim. Acta 282 (1999) 115–123.
[72] C. Murr, A. Bergant, M. Widschwendter, K. Heim, H. Schrocksnadel, D. Fuchs, Neopterin is an independent prognostic variable in females with breast cancer, Clin. Chem. 45 (1999) 1998–2004.
[73] E.R. Werner, A. Bichler, G. Daxenbichler, D. Fuchs, L.C. Fuith, A. Hausen, H. Hetzel, G. Reibnegger, H. Wachter, Determinatiuon of neopterin in serum and urine, Clin. Chem. 33 (1987) 62–66.
[74] A. Shrivastava, V. Gupta, Methods for the determination of limit of detection and limit of quantitation of the analytical methods, Chronicles of Young Scientists, 2 2011, pp. 21–25.